frontiers | Frontiers in Chemistry

TYPE Original Research
PUBLISHED 09 January 2024
DOI 10.3389/fchem.2023.1306495

OPEN ACCESS

EDITED BY
Maxim Bykov,
University of Cologne, Germany

REVIEWED BY
Guo-Hua Zhong,
Chinese Academy of Sciences (CAS), China
Marek Tkacz,
Institute of Physical Chemistry, Polish Academy of Sciences, Poland

*CORRESPONDENCE
Miriam Peña-Alvarez,
miriam.pena.alvarez@ed.ac.uk

RECEIVED 03 October 2023
ACCEPTED 19 December 2023
PUBLISHED 09 January 2024

CITATION
Marqueño T, Kuzovnikov MA, Osmond I, Dalladay-Simpson P, Hermann A, Howie RT and Peña-Alvarez M (2024), High pressure study of sodium trihydride. *Front. Chem.* 11:1306495. doi: 10.3389/fchem.2023.1306495

High pressure study of sodium trihydride

Tomas Marqueño[1], Mikhail A. Kuzovnikov[1], Israel Osmond[1], Phillip Dalladay-Simpson[2], Andreas Hermann[1], Ross T. Howie[1,2] and Miriam Peña-Alvarez[1]*

[1]Centre for Science at Extreme Conditions (CSEC), The School of Physics and Astronomy, The University of Edinburgh, Edinburgh, United Kingdom, [2]Center for High Pressure Science and Technology Advanced Research, Shanghai, China

The reactivity between NaH and H_2 has been investigated through a series of high-temperature experiments up to pressures of 78 GPa in diamond anvil cells combined with *first principles* calculations. Powder X-ray diffraction measurements show that heating NaH in an excess of H_2 to temperatures around 2000 K above 27 GPa yields sodium trihydride (NaH_3), which adopts an orthorhombic structure (space group *Cmcm*). Raman spectroscopy measurements indicate that NaH_3 hosts quasi-molecular hydrogen ($H_2^{\delta-}$) within a NaH lattice, with the $H_2^{\delta-}$ stretching mode downshifted compared to pure H_2 ($\Delta\nu$ ~−120 cm^{-1} at 50 GPa). NaH_3 is stable under room temperature compression to at least 78 GPa, and exhibits remarkable *P-T* stability, decomposing at pressures below 18 GPa. Contrary to previous experimental and theoretical studies, heating NaH (or NaH_3) in excess H_2 between 27 and 75 GPa does not promote further hydrogenation to form sodium polyhydrides other than NaH_3.

KEYWORDS

hydrides, sodium, high pressure, X-ray diffraction, Raman, density functional calculations

1 Introduction

The synthesis of metallic alloys hosting hydrogen at high pressures has attracted significant interest, especially after the suggestion of their potential high-temperature superconductivity (Ashcroft, 2004). This was demonstrated by the pioneering work on LaH_{10} with a critical temperature (T_c) of T_c = 250 K at 170 GPa (Drozdov et al., 2019; Somayazulu et al., 2019). However, there are essential aspects of high pressure hydrides that must be understood in order to provide an efficient route towards desired target properties. The alkali metal lithium was one of the first systems studied as a promising hydrogen host for superconductivity (Zurek et al., 2009). However, experimentally these compounds have proven difficult to synthesize, with some spectroscopic evidence that LiH reacts with H_2 and transforms into LiH_2 and LiH_6 above 130 GPa hosting molecular hydrogen, which would prevent any favorable electron phonon coupling (Howie et al., 2012; Pépin et al., 2015).

Subsequent *first principles* simulations predicted that all of the heavier alkali metals could form highly stoichiometric hydrides (Baettig and Zurek, 2011; Hooper and Zurek, 2012; Shamp et al., 2012; Hooper et al., 2013; Shipley et al., 2021). Some of them such as KH_n with $n > 1$ could also form stable polyhydrides at pressures as low as 3 GPa (Hooper and Zurek, 2012). Despite these theoretical predictions, only the hydrides of lithium (Pépin et al., 2015) and sodium (Struzhkin et al., 2016) have been experimentally approached. This is due to the experimental difficulties arising from studying alkali elements, which instantly react with the

oxygen and water present in the atmosphere. The high reactivity of the alkali metals is the cause why there are very few studies on their polyhydrides.

Structural searches suggest that alkali metal polyhydrides are some of the best candidates for high T_c superconductivity among all possible binary hydrides (Shipley et al., 2021), with high predicted T_c values at lower pressures than those required for previously observed superconducting rare earth hydrides. In particular, superconductivity is predicted in Na_2H_{11} (T_c ~ 150 K at 100 GPa) and in NaH_6, where T_c predictions range from 180 to 260 K at 50 and 100 GPa respectively (Chen et al., 2021; Shipley et al., 2021). The Na-H system has previously been studied experimentally up to 50 GPa, forming NaH_3 (*Cmcm*) and NaH_7 (*Cc*) above 40 GPa and 2000 K Struzhkin et al. (2016). Analogous to the lithium polyhydrides, NaH_3 and NaH_7 have been described to host quasi-molecular hydrogen. Thus, the sodium-hydrogen system remains experimentally unexplored above 50 GPa.

In this work, we explore the reactivity of the NaH-H_2 system up to pressures of ~ 78 GPa and temperatures in excess of 2000 K using X-ray diffraction (XRD) and Raman spectroscopy diagnostics, combined with *first principles* calculations. Laser heating NaH in an excess H_2 medium at pressures above 27 GPa yields *Cmcm*-NaH_3, which remains the only product up to pressures of 78 GPa. The Raman spectrum of NaH_3 is dominated by an intense mode (at ~ 4120 cm^{-1}) related to the intramolecular stretching modes of quasi-molecular $H_2^{\delta-}$ units within the NaH_3 structure. Relative to pure H_2 (Sharma et al., 1980; Howie et al., 2013), this mode is at lower frequencies, and upshifts monotonically in frequency up to 75 GPa, indicating a shortening of the H-H bonds, with no evidence of change in its pressure-frequency dependence. NaH_3 exhibits remarkable pressure-temperature stability, decomposing into hydrogen and sodium monohydride upon room temperature decompression below 18 GPa.

2 Experimental details

Diamond anvil cells were prepared with diamond culet sizes of 80–200 μm, with the sample chamber formed by pre-indentation and laser drilling of a Re gasket. Sodium monohydride (Sigma Aldrich, 95% dry) was loaded into the sample chambers in an inert argon atmosphere glove box to prevent the oxidation of NaH. This was loaded together with small grains of gold powder used as a pressure calibrant for XRD experiments (Fei et al., 2007). The DACs were subsequently loaded with research grade (99.9999%) hydrogen gas at 2000 bar. The samples were heated using a 1,064 nm YAG laser. A summary of the experiments performed with each sample is given in Supplementary Table S1 in the Supplementary Data.

The XRD measurements were performed at the Sector 13 (GSECARS) beamline at the Advanced Photon Source (ANL, United States) (Shen et al., 2005; Prakapenka et al., 2008) and the P02.2 Extreme Conditions Beamline at PETRA-III (DESY, Germany) (Liermann et al., 2015). The relevant details of the beamline regarding our experiments are summarized in Supplementary Table S2 (Supplementary Data). The integration of the XRD patterns was performed using DIOPTAS (Prescher and Prakapenka, 2015). The analysis and refinement of the obtained XRD patterns were carried out using the software packages PowderCell and GSAS-II (Kraus and Nolze, 1996; Toby and Von Dreele, 2013).

Raman measurements of the samples were acquired using a custom-built confocal microfocused Raman setup with 514.5 nm Ar-ion laser excitation source, equipped with a PyLoN: 100 cryogenically cooled CCD camera (1,340 × 100 sensor). In order to measure Raman spectra in a wide range of frequencies, a grating of 300 lines/mm was used. Pressure was monitored in Raman measurements using the frequency of the vibron of excess H_2 (Howie et al., 2013), and cross-checked with the frequency of the stressed Raman edge of diamond (Akahama and Kawamura, 2006).

3 Computational details

Total energy density functional theory calculations were performed with the VASP package, using plane wave basis sets in conjunction with projector augmented wave (PAW) atomic data sets (Kresse and Furthmüller, 1996; Kresse and Joubert, 1999). The plane wave energy cutoff was 800 eV, Brillouin zone sampling used regular grids with linear k-point densities of 40/Å^{-1}, and 'hard' PAW datasets that consider the $1s^1/2s^22p^63s^1$ states as valence electrons, and have cutoff radii 0.8/2.2 Bohrs for H/Na, respectively. The structures were fully optimized over a range of pressures between 10 and 90 GPa, and until all atomic force components were below 1 meV/Å. Electronic exchange-correlation effects were described within the generalized gradient approximation, using the Perdew–Burke–Ernzerhof (PBE) parameterization (Perdew et al., 1996) and, for comparison, the semi-empirical Grimme D3 dispersion correction (Grimme et al., 2011) as well as the nonlocal vdW-DF optB88-vdW functional (Klimeš et al., 2010) (Supplementary Data, Supplementary Figure S1). Phonon calculations were performed using the finite-displacement method in suitable supercells of all Na-H compounds considered here (see Supplementary Material for details, Supplementary Figure S2); they were set up and analyzed using the phonopy and phonopy-spectroscopy packages (Togo and Tanaka, 2015; Skelton et al., 2017). Reaction enthalpies between NaH, NaH_6, H_2 to form NaH_3 are shown in Supplementary Figure S3 (Supplementary Data).

4 Results

4.1 X-ray diffraction experiments

At room pressure and temperature, sodium hydride (NaH-I) crystallizes in a *fcc* structure analogous to that of NaCl (rock salt), in which hydrogen atoms occupy octahedral interstitial sites (Shull et al., 1948). Above ~ 30 GPa, NaH undergoes a phase transition from a *fcc* to a CsCl-type (simple cubic, NaH-II) structure (Duclos et al., 1987). Both NaH-I and II contain atomic hydrogen, which partially forms ionic bonds with sodium. The unit-cells of these NaH-I and II structures are shown in Figures 1A, B respectively.

NaH in H_2 was compressed to 50 GPa and we did not observe the formation of any higher hydride with a larger hydrogen content, as shown in the bottom panel of 2 a). Since there are likely to be

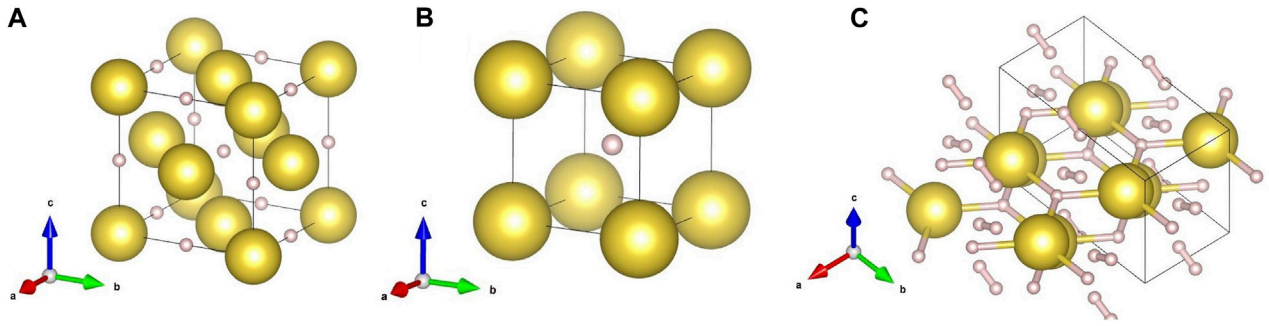

FIGURE 1
Relevant crystal structures of the Na-H system in our study: **(A)** NaH-I ($Fm\bar{3}m$), **(B)** NaH-II ($Pm\bar{3}m$) and **(C)** NaH_3 ($Cmcm$). Yellow and white spheres represent Na and H atoms, respectively. The structures were taken from Shull et al. (1948), Duclos et al. (1987) and Struzhkin et al. (2016).

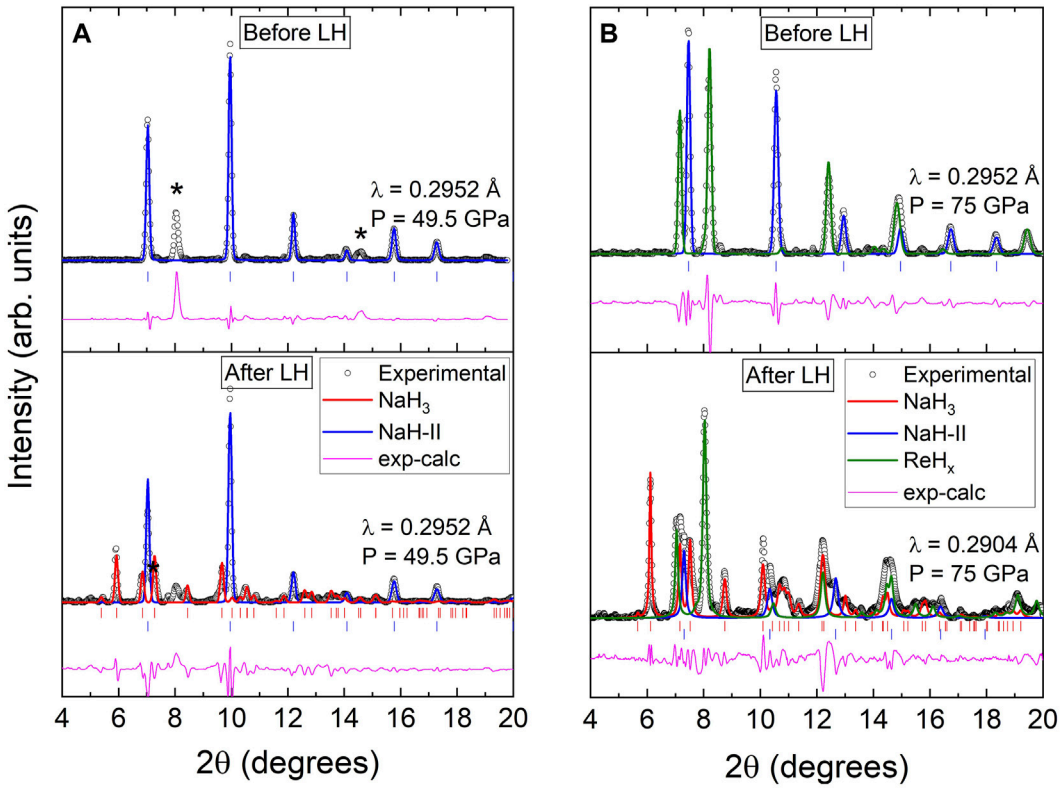

FIGURE 2
(A) & **(B)** Powder XRD pattern and LeBail refinements of two different samples before and after laser heating at 49.5 GPa and 75 GPa, respectively. Experimental data is represented by circles. The calculated contributions from NaH-II, *Cmcm*-NaH_3 and hcp-ReH_x phases are shown by the blue, red, and green curves, respectively. The reflections corresponding to NaH_3 and NaH are indicated with red and blue ticks respectively. Asterisks in **(A)** indicate reflections associated with ReH_x.

energy barriers preventing the chemical reaction between NaH and H_2, we laser heated our sample at ~ 50 GPa until thermal emission was visible. The estimated maximum temperatures on the laser-heated surface range from 1,500 to 2100 K, according to the thermal emission of blackbody radiation from the sample. As shown in Figure 2A, the quenched sample is mainly composed of non-reacted NaH-I (*fcc*) and a second phase which we identify as *Cmcm*-NaH_3. The unit-cell of NaH_3 is shown in Figure 1C. NaH_3 has a distorted hexagonal close-packed (*hcp*) lattice of sodium atoms. According to the DFT-based *first principles* predictions (Struzhkin et al., 2016), the hydrogen in NaH_3 is present in the form of H^- anions with planar triangular coordination within the *hcp* planes of metal atoms, and $H_2^{\delta-}$ quasi-molecular units filling the octahedral interstitial sites. At 49.5 GPa, the lattice parameters of NaH_3 after the LeBail

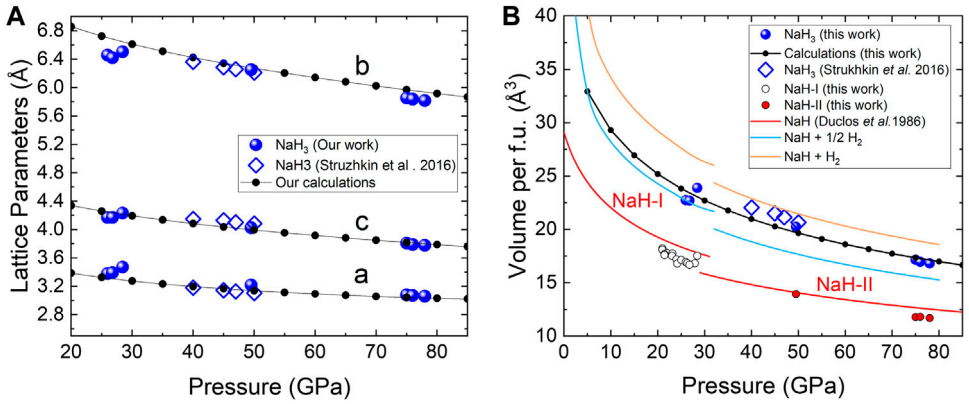

FIGURE 3
Pressure dependence of the **(A)** lattice parameters and **(B)** volume per formula unit of NaH_3. The data obtained in our experiments is represented with blue spheres; small connected black dots stand for the results of our calculations. The data reported by Struzhkin et al. (2016) is depicted with diamonds. The red solid line stands for the volume-pressure curves of NaH (phases I and II) reported by Duclos et al. (1987). Blue and orange solid lines stand for the volume sums $V(\mathrm{NaH}) + \frac{1}{2}V(\mathrm{H_2})$ and $V(\mathrm{NaH}) + V(\mathrm{H_2})$, respectively (Duclos et al., 1987; Loubeyre et al., 1996).

refinement are $a = 3.218$ Å, $b = 6.251$ Å and $c = 4.027$ Å ($V_{\mathrm{f.u.}} = 20.25$ Å^3). The evolution of the lattice parameters and unit-cell volume are in reasonably good agreement with the observations reported by Struzhkin et al. (2016) and our own DFT calculations (Figure 3). As further verification for the NaH_3 stoichiometry, we estimate the minimum amount of hydrogen using the Le Châtelier principle regarding volume change:

$$V(\mathrm{NaH}_n) \leq V(\mathrm{NaH}) + (n-1)V\left(\frac{1}{2}\mathrm{H_2}\right) \quad (1)$$

in which we can use the volumes of NaH and H_2 reported in the literature (Duclos et al., 1987; Loubeyre et al., 1996). The sum of the individual volumes per formula unit (f.u.) of NaH and H_2 is displayed in Figure 3B for n = 1, 2 and 3 (Eq. 1). Experimental volumes are above and below the curves corresponding to $n = 2$ and 3, respectively. Thus, both XRD patterns and experimental volumes support the assignment to *Cmcm*-NaH_3.

To investigate the stability range of NaH_3, we heated subsequent samples below 50 GPa to temperatures in excess of 2000 K, where synthesis could be achieved as low as 30 GPa (see Supplementary Figure S4 in the Supplementary Data). Heating NaH + H_2 at 75 GPa to similar temperatures converted a greater proportion of NaH to NaH_3 than heating at either 27 GPa or 49.5 GPa. This could indicate greater stability and lower kinetic barriers to formation at higher pressure, but could also be due to differences in sample morphology. However, we did not observe any signatures of any other polyhydride compounds upon laser heating in the 30–75 GPa pressure range, with traces of the already reported NaH_7 polyhydride (Struzhkin et al., 2016). These results agree with our theoretical predictions, which indicate that within the experimentally explored conditions NaH_3 should form from NaH and H_2, irrespective of exchange-correlation functional used (Supplementary Data, Supplementary Figures S1–S3). In the case of recently suggested NaH_6 (Chen et al., 2021; Shipley et al., 2021), our calculations suggest that this polyhydride should react with NaH to form NaH_3 at any pressure below 100 GPa (Supplementary Figure S3).

4.2 Raman scattering experiments

Prior to the heating of the sample, NaH-II exhibited no Raman activity, as it is shown in Supplementary Figure S6 (Supplementary Data) for a sample at ~ 50 GPa. After laser heating, the Raman spectrum changes significantly, with intense activity attributed to the formation of NaH_3. Figures 4A, B show the spectra of different samples of NaH_3 at different pressures. The spectral distribution of the modes is in good agreement with our simulated Raman spectra for NaH_3, which are shown in Figure 4C. Remarkably, the Raman signatures of NaH_3 are experimentally observed down to 18 GPa upon decompression, with the absence of any Raman activity below this pressure suggesting that the decomposition products are NaH and H_2.

At frequencies below 1,200 cm^{-1}, the Raman spectrum of NaH_3 at 75 GPa is characterized by an intense, sharp mode at ~ 250 cm^{-1}, together with a lower intensity satellite mode at ~ 300 cm^{-1} and a broad band at ~ 800 cm^{-1}. Our DFT calculations relate the first two bands to a B_g mode, and to the overlap of an A_g and B_{3g} modes respectively. Both bands are then associated with Na and atomic H displacements in opposite directions coupled to one H_2 libration. The broad band at ~ 800 cm^{-1} can be ascribed to the overlap of four Raman modes: B_{3g}, B_{1g}, B_{2g} and A_g. These modes involve both librational and translational vibrations of the quasi-molecular $H_2^{\delta-}$ units, coupled with displacements of the atomic hydrogen, while the Na atoms remain almost stationary. On decompression, below 30 GPa, we observe the growth of wide contributions between 1,000 and 1,300 cm^{-1}, Figure 4A. Our XRD results do not show any symmetry change due to possible structural transitions in NaH_3, which remains *Cmcm* down to 18 GPa, Therefore, since these new bands appear after the transition from NaH-II (*sc*) to NaH-I (*fcc*), they could be related to second-order Raman modes of NaH-I, similar to those observed

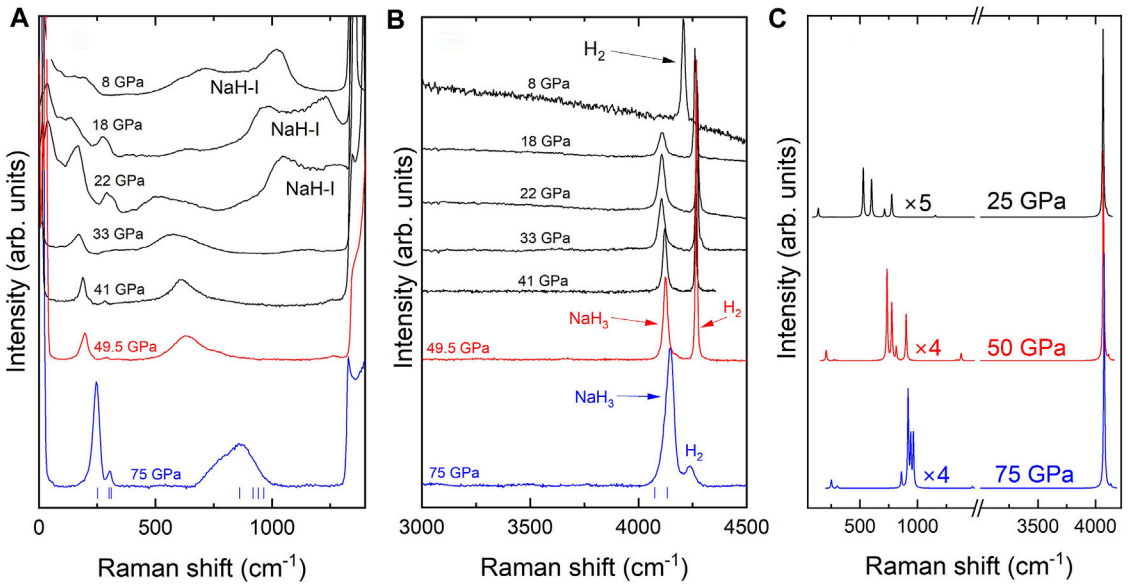

FIGURE 4
(A,B) Raman spectra of NaH_3 samples. Blue and red solid lines correspond to NaH_3 samples at 75 and 49.5 GPa, respectively, which were discussed in Figure 2. The black solid lines correspond to a different Raman experiment on NaH_3 upon decompression from 41 to 8 GPa. Blue vertical ticks represent the simulated Raman frequencies of NaH_3 at 75 GPa. **(C)** Simulated Raman spectra of NaH_3 at 75, 50 and 25 GPa (blue, red and black lines, respectively). The peak intensities of the spectra below 1,500 cm^{-1} have been magnified by the indicated factors.

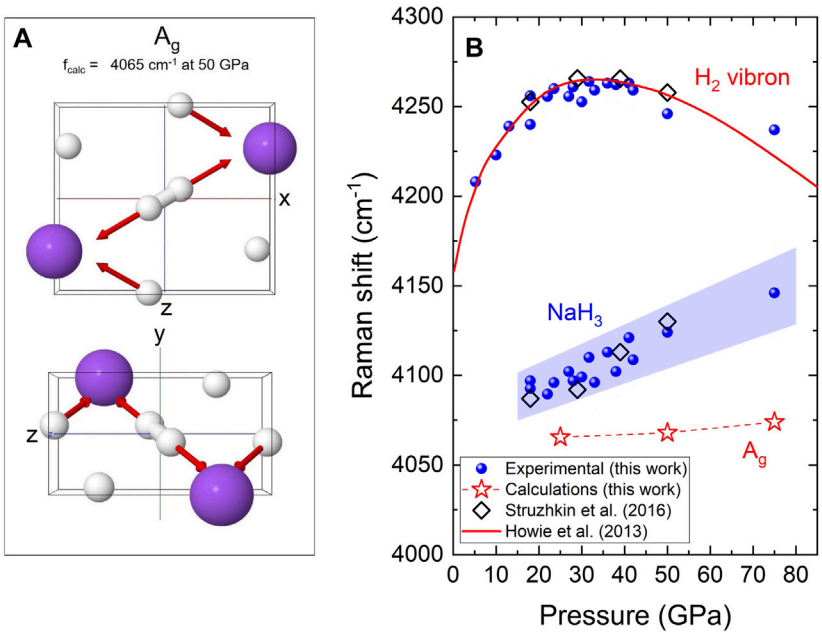

FIGURE 5
(A) Eigenmode corresponding to the $H_2^{\delta-}$ vibron of NaH_3 under different perspectives according to primitive unit-cell coordinates. Na and H atoms are represented by purple and white spheres, respectively. The red arrow represents the motion associated with each atom. The calculated frequency f_{calc} is 4,065 cm^{-1} at 50 GPa. **(B)** Pressure evolution of the vibron frequencies of H_2 and NaH_3. Our experimental data is represented with blue spheres, with the area shaded in blue depicting the FWHM of the peaks associated with NaH_3. Calculated data is shown with connected stars. Dashed lines are for visual guidance. Diamonds represent the experimental data reported by Struzhkin et al. (2016). The pressure evolution of the pure H_2 vibron reported by Howie et al. (2013) is shown as a solid red line.

in isomorphic LiH (*fcc*), so we labelled them as "NaH-I". (Ho et al., 1997; Howie et al., 2012).

At high frequency, the Raman spectrum of NaH_3 is dominated by an intense mode at 4,145 cm^{-1} (at 75 GPa), which is directly related to the H-H stretching vibrations from quasi-molecular $H_2^{\delta-}$ units in NaH_3. In hydride systems containing H_2 units, the surrounding metallic lattice and the resulting charge transfer leads to modified H-H bond lengths when compared to that of pure hydrogen, causing a frequency downshift in the $H_2^{\delta-}$ vibron (Peña-Alvarez et al., 2022). In this frequency regime, two Raman modes are predicted to be present at similar frequencies, A_g and B_{3g}. However the intensity of the B_{3g} is expected to be significantly lower, i.e., $I(B_{3g})/I(A_g)$ ~ 1.2%, according to our calculations. The eigenmode of the A_g vibration is depicted in Figure 5A showing its correspondence to the H-H stretching mode.

Interestingly, some NaH samples exhibited an intense photoluminescence background signal after exposure to X-ray radiation and IR laser used for heating. This can be attributed to the formation of color centers, which have previously been observed in studies of pure NaH Duclos et al. (1987); Williams (1962) and reported for isoelectronic alkaline halides such as NaF (Bryukvina et al., 2014). Furthermore, whilst the samples undergo a visual color change, appearing orange after X-ray irradiation at 75 GPa (Supplementary Figure S5B [Supplementary Data]), XRD mapping of the samples showing this photoluminescence did not reveal the formation of any other product or phase transition.

Figure 5B presents the Raman shift as a function of pressure of the NaH_3 $H_2^{\delta-}$ vibron, from our experimental and theoretical results, together with that of pure H_2 (Howie et al., 2013). Comparing the Raman spectra of NaH_3 and H_2, we observe that the quasi-molecular $H_2^{\delta-}$ vibron is at lower frequencies than that of pure hydrogen. For instance, at 50 GPa in NaH_3 the $H_2^{\delta-}$ vibron is at 4,124 cm^{-1}, whereas in pure H_2 the vibron is at 4,246 cm^{-1} ($\Delta\nu = -122$ cm^{-1}). It is known that the compression of hydrogen leads to an initial upshift of its vibron, up to a maximum at 30–40 GPa, after which intermolecular interactions lead to a vibron downshift upon further compression (Sharma et al., 1980; Howie et al., 2012; Howie et al., 2013). In NaH_3, however, the $H_2^{\delta-}$ vibron monotonically upshifts upon compression, going from 4,092 cm^{-1} at 18 GPa to 4,146 cm^{-1} at 75 GPa. This indicates that, in contrast to pure H_2, pressure does not favor the lengthening of the H-H bond in NaH_3, which is responsible for the eventual vibron downshift in pure hydrogen.

Similar behavior is also observed in previous measurements on the lithium-hydride system. IR absorption measurements show that while the vibron of pure H_2 is located at around 4,450 cm^{-1} at 240 GPa (Zha et al., 2013), the vibrons of LiH_2 and LiH_6 are around 3900 cm^{-1} and 2,600 cm^{-1} at 160 GPa, respectively (Pépin et al., 2015). Like NaH_3, these vibrons in LiH_2 and LiH_6 display a positive frequency shift with pressure. For instance, in LiH_2 the vibron upshifts from 3900 at 160 GPa to 4,250 cm^{-1} at 220 GPa. These results contrast with the experimental observations on alkaline earth tetrahydrides (MH_4 with M = Ca, Sr, Ba) which also contain quasi-molecular hydrogen (Peña-Alvarez et al., 2022). In these tetrahydrides, the frequency of the $H_2^{\delta-}$ vibron downshifts upon compression, which is directly related to a progressive elongation of the intramolecular bond.

The pressure induced H-H lengthening in binary hydrides has been suggested to be directly related to the charge transfer from the host element to the $H_2^{\delta-}$ unit, populating the σ^* orbitals (Wang et al., 2012; Bi and Zurek, 2021). This would lead to an increase in the repulsion of the anti-bonding orbitals and the subsequent weakening of the bond. However, more recent studies have shown that the stretching of the H-H bond under compression results from a combination of charge transfer and the confinement of the molecule to small interstitial locations (Peña-Alvarez et al., 2022).

TABLE 1 Calculated average charges for sodium, quasi-molecular and atomic hydrogen inside of the *Cmcm*-NaH_3 structure at different pressures.

Pressure (GPa)	Na	$H_2^{\delta-}$ units	Atomic H
25	+0.7842	−0.1153	−0.6690
50	+0.7669	−0.1173	−0.6496
75	+0.7490	−0.1216	−0.6274

According to our calculations, shown in Table 1, the charge of the Na cation goes from +0.7842 at 25 GPa to +0.7490 at 75 GPa. Similarly, the charge of the H anions goes from −0.6690 to −0.6274 at 25 and 75 GPa, respectively. Thus, most of the charge is transferred from sodium to the monoatomic hydrogen, while there is some charge on the $H_2^{\delta-}$ quasi-molecular units, which remains almost constant over this pressure range (δ ~ 0.12). With very little charge transfer into the $H_2^{\delta-}$ units, there is no substantial increase in the occupation of the antibonding states of the $H_2^{\delta-}$ units, which is compatible with the shortening of the H-H quasi-molecular bond upon compression. Factors such as the relative arrangement of the elements within the crystal structure and the size of the cation are also expected to play an important role in the observed pressure dependence (Peña-Alvarez et al., 2022). For example, in NaH_3, the $H_2^{\delta-}$ units are located between hexagonal layers of Na-H, whereas in alkali-earth tetrahydrides $H_2^{\delta-}$ units occupy the interstitial positions of 3D-compact network structures (Peña-Alvarez et al., 2022). Therefore, our observations on the quasi-molecular Raman vibron of NaH_3 can be justified by 1) the constant charge of the $H_2^{\delta-}$ units and 2) the location of the $H_2^{\delta-}$ units between Na-H layers.

The results presented here show that the previous study on the Na-H misinterpreted their Raman spectra by attributing the characteristic A_g mode of *Cmcm*-NaH_3 to *Cc*-NaH_7 (Struzhkin et al., 2016). Furthermore, the Raman modes assigned to NaH_3 by Struzhkin et al. (2016) can be explained by the formation of CH_4-H_2 compounds from the high temperature reaction between the diamond anvil and the H_2 medium (Peña-Alvarez et al., 2021; Ranieri et al., 2022). Our XRD and Raman results provide no evidence for the existence of *Cc*-NaH_7 in the 25–75 GPa pressure range, which is within the synthesis conditions previously reported. We can as well rule out the formation of any of the predicted sodium polyhydrides (Baettig and Zurek, 2011; Chen et al., 2021; Shipley et al., 2021), to at least 78 GPa.

5 Conclusion

We have synthesized NaH_3 from NaH and H_2 at the high hydrogen pressures of ~ 30, 40, 50 and 75 GPa and temperatures of 2000 K using laser heating. XRD measurements at 27, 49.5 and

75 GPa show that the crystal structure of the metal sublattice of NaH_3 is compatible with the orthorhombic space group *Cmcm*. The Na volume expansion corresponds to a NaH_3 stoichiometry. The unit-cell lattice parameters and unit-cell volume experimental points as a function of pressure are in good agreement with our DFT calculations for NaH_3 and the previously reported data below 50 GPa (Struzhkin et al., 2016). Different and independent samples of NaH_3 at 75 and 50 GPa were measured by Raman spectroscopy. Further Raman experiments were performed on an additional sample to characterize NaH_3 upon decompression from 41 to 8 GPa. The NaH_3 Raman spectrum is characterized by a phonon near 4,125 cm^{-1} (~ 50 GPa), assigned to the stretching vibration of quasi-molecular $H_2^{\delta-}$ units trapped inside of the structure, visible at lower frequencies than that of pure H_2. In contrast to pure H_2, the stretching mode from $H_2^{\delta-}$ units in NaH_3 upshifts during compression, indicating that chemical pre-compression is not favored. Despite several experimental attempts, we were unable to identify any sodium polyhydride with a hydrogen content higher than NaH_3, suggesting that NaH_3 may be the only stable hydride below 78 GPa.

Data availability statement

The raw data supporting the conclusion of this article will be made available by the authors, without undue reservation.

Author contributions

TM: Conceptualization, Data curation, Formal Analysis, Investigation, Methodology, Writing–original draft, Writing–review and editing. MK: Data curation, Investigation, Writing–review and editing, Formal Analysis. IO: Investigation, Methodology, Writing–review and editing, Validation. PD-S: Investigation, Writing–review and editing. AH: Formal Analysis, Investigation, Methodology, Resources, Software, Validation, Writing–review and editing. RH: Funding acquisition, Investigation, Methodology, Resources, Supervision, Writing–review and editing, Validation. MP-A: Conceptualization, Data curation, Formal Analysis, Funding acquisition, Investigation, Methodology, Project administration, Resources, Supervision, Validation, Writing–original draft, Writing–review and editing.

Funding

The author(s) declare financial support was received for the research, authorship, and/or publication of this article. MP-A acknowledges the support of the UKRI Future Leaders Fellowship Mrc-Mr/T043733/1. RH acknowledges that the project has received funding from the European Research Council (ERC) under the European Union's Horizon 2020 Research and Innovation program (Grant Agreement No. 948895).

Acknowledgments

We thank Prof. M. McMahon for lending us the glove box of his laboratory to prepare the samples. We also thank beamline P02.2 at PETRA-III, DESY, Hamburg, Germany for the use of their facilities (proposal I-20221042) as well as beamline scientists Nico Giordano, Konstantin Glazyrin and Hanns-Peter Lierman for their help during the experiments. We would also like to acknowledge beamline 13 IDD–GSECARS in the Advance Photon Source (APS) at the Argonne National Laboratory, Illinois, United States, for granting us beamtime (experiments ID 266009, 216253, 208124, and 179388). Beamline scientists Stella Chariton and Vitali Prakapenka are also thanked for their help. We also would like to acknowledge Jack Binns for his help during data analysis and Prof. Eugene Gregoryanz for facilitating the equipment for the experiments. Computational resources provided by the UK's National Supercomputer Service through the United Kingdom Car-Parrinello HEC consortium (EP/X035891/1) and by the United Kingdom Materials and Molecular Modelling Hub (EP/P020194) are gratefully acknowledged.

Conflict of interest

The authors declare that the research was conducted in the absence of any commercial or financial relationships that could be construed as a potential conflict of interest.

Publisher's note

All claims expressed in this article are solely those of the authors and do not necessarily represent those of their affiliated organizations, or those of the publisher, the editors and the reviewers. Any product that may be evaluated in this article, or claim that may be made by its manufacturer, is not guaranteed or endorsed by the publisher.

Supplementary material

The Supplementary Material for this article can be found online at: https://www.frontiersin.org/articles/10.3389/fchem.2023.1306495/full#supplementary-material

References

Akahama, Y., and Kawamura, H. (2006). Pressure calibration of diamond anvil Raman gauge to 310 GPa. *J. Appl. Phys.* 100. doi:10.1063/1.2335683

Ashcroft, N. (2004). Hydrogen dominant metallic alloys: high temperature superconductors? *Phys. Rev. Lett.* 92, 187002. doi:10.1103/physrevlett.92.187002

Baettig, P., and Zurek, E. (2011). Pressure-stabilized sodium polyhydrides: NaH_n ($n > 1$). *Phys. Rev. Lett.* 106, 237002. doi:10.1103/physrevlett.106.237002

Bi, T., and Zurek, E. (2021). Electronic structure and superconductivity of compressed metal tetrahydrides. *Chem. Eur. J.* 27, 14858–14870. doi:10.1002/chem.202102679

Bryukvina, L., Pestryakov, E., Kirpichnikov, A., and Martynovich, E. (2014). Formation of color centers and light scattering structures by femtosecond laser pulses in sodium fluoride. *Opt. Commun.* 330, 56–60. doi:10.1016/j.optcom.2014.05.030

Chen, C.-H., Huang, A., Tsuei, C., and Jeng, H.-T. (2021). Possible high-T_c superconductivity at 50 GPa in sodium hydride with clathrate structure. *New J. Phys.* 23, 093007. doi:10.1088/1367-2630/ac1df3

Drozdov, A., Kong, P., Minkov, V., Besedin, S., Kuzovnikov, M., Mozaffari, S., et al. (2019). Superconductivity at 250 K in lanthanum hydride under high pressures. *Nature* 569, 528–531. doi:10.1038/s41586-019-1201-8

Duclos, S. J., Vohra, Y. K., Ruoff, A. L., Filipek, S., and Baranowski, B. (1987). High-pressure studies of NaH to 54 GPa. *Phys. Rev. B* 36, 7664–7667. doi:10.1103/physrevb.36.7664

Fei, Y., Ricolleau, A., Frank, M., Mibe, K., Shen, G., Prakapenka, V., et al. (2007). Toward an internally consistent pressure scale. *Proc. Natl. Acad. Sci* 104 (22), 9182–9186. doi:10.1073/pnas.0609013104

Grimme, S., Ehrlich, S., and Goerigk, L. (2011). Effect of the damping function in dispersion corrected density functional theory. *J. Comput. Chem.* 32, 1456–1465. doi:10.1002/jcc.21759

Ho, A. C., Hanson, R. C., and Chizmeshya, A. (1997). Second-order Raman spectroscopic study of lithium hydride and lithium deuteride at high pressure. *Phys. Rev. B* 55, 14818–14829. doi:10.1103/physrevb.55.14818

Hooper, J., Altintas, B., Shamp, A., and Zurek, E. (2013). Polyhydrides of the alkaline earth metals: a look at the extremes under pressure. *J. Phys. Chem. C* 117, 2982–2992. doi:10.1021/jp311571n

Hooper, J., and Zurek, E. (2012). High pressure potassium polyhydrides: a chemical perspective. *J. Phys. Chem. C* 116, 13322–13328. doi:10.1021/jp303024h

Howie, R. T., Gregoryanz, E., and Goncharov, A. F. (2013). Hydrogen (deuterium) vibron frequency as a pressure comparison gauge at multi-mbar pressures. *J. Appl. Phys.* 114. doi:10.1063/1.4818606

Howie, R. T., Narygina, O., Guillaume, C. L., Evans, S., and Gregoryanz, E. (2012). High-pressure synthesis of lithium hydride. *Phys. Rev. B* 86, 064108. doi:10.1103/physrevb.86.064108

Klimeš, J., Bowler, D. R., and Michaelides, A. (2010). Chemical accuracy for the van der Waals density functional. *J. Phys. Condens. Matter* 22, 022201. doi:10.1088/0953-8984/22/2/022201

Kraus, W., and Nolze, G. (1996). Powder cell–a program for the representation and manipulation of crystal structures and calculation of the resulting x-ray powder patterns. *J. Appl. Crystallogr.* 29, 301–303. doi:10.1107/s0021889895014920

Kresse, G., and Furthmüller, J. (1996). Efficient iterative schemes for *ab initio* total-energy calculations using a plane-wave basis set. *Phys. Rev. B* 54, 11169–11186. doi:10.1103/physrevb.54.11169

Kresse, G., and Joubert, D. (1999). From ultrasoft pseudopotentials to the projector augmented-wave method. *Phys. Rev. B* 59, 1758–1775. doi:10.1103/physrevb.59.1758

Liermann, H.-P., Konôpková, Z., Morgenroth, W., Glazyrin, K., Bednarčik, J., McBride, E., et al. (2015). The extreme conditions beamline P02.2 and the extreme conditions science infrastructure at PETRA III. *J. Synchrotron Radiat.* 22, 908–924. doi:10.1107/s1600577515005937

Loubeyre, P., LeToullec, R., Hausermann, D., Hanfland, M., Hemley, R., Mao, H., et al. (1996). X-ray diffraction and equation of state of hydrogen at Megabar pressures. *Nature* 383, 702–704. doi:10.1038/383702a0

Peña-Alvarez, M., Binns, J., Marqués, M., Kuzovnikov, M. A., Dalladay-Simpson, P., Pickard, C. J., et al. (2022). Chemically assisted precompression of hydrogen molecules in alkaline-earth tetrahydrides. *J. Phys. Chem. Lett.* 13, 8447–8454. doi:10.1021/acs.jpclett.2c02157

Peña-Alvarez, M., Brovarone, A. V., Donnelly, M.-E., Wang, M., Dalladay-Simpson, P., Howie, R., et al. (2021). *In-situ* abiogenic methane synthesis from diamond and graphite under geologically relevant conditions. *Nat. Commun.* 12, 6387. doi:10.1038/s41467-021-26664-3

Pépin, C., Loubeyre, P., Occelli, F., and Dumas, P. (2015). Synthesis of lithium polyhydrides above 130 GPa at 300 K. *Proc. Natl. Acad. Sci.* 112, 7673–7676. doi:10.1073/pnas.1507508112

Perdew, J. P., Burke, K., and Ernzerhof, M. (1996). Generalized gradient approximation made simple. *Phys. Rev. Lett.* 77, 3865–3868. doi:10.1103/physrevlett.77.3865

Prakapenka, V., Kubo, A., Kuznetsov, A., Laskin, A., Shkurikhin, O., Dera, P., et al. (2008). Advanced flat top laser heating system for high pressure research at GSECARS: application to the melting behavior of germanium. *High. Press. Res.* 28, 225–235. doi:10.1080/08957950802050718

Prescher, C., and Prakapenka, V. B. (2015). Dioptas: a program for reduction of two-dimensional x-ray diffraction data and data exploration. *High. Press. Res.* 35, 223–230. doi:10.1080/08957959.2015.1059835

Ranieri, U., Conway, L. J., Donnelly, M.-E., Hu, H., Wang, M., Dalladay-Simpson, P., et al. (2022). Formation and stability of dense methane-hydrogen compounds. *Phys. Rev. Lett.* 128, 215702. doi:10.1103/physrevlett.128.215702

Shamp, A., Hooper, J., and Zurek, E. (2012). Compressed cesium polyhydrides: Cs^+ sublattices and H^{3-}-three-connected nets. *Inorg. Chem.* 51, 9333–9342. doi:10.1021/ic301045v

Sharma, S., Mao, H., and Bell, P. (1980). Raman measurements of hydrogen in the pressure range 0.2-630 kbar at room temperature. *Phys. Rev. Lett.* 44, 886–888. doi:10.1103/physrevlett.44.886

Shen, G., Prakapenka, V. B., Eng, P. J., Rivers, M. L., and Sutton, S. R. (2005). Facilities for high-pressure research with the diamond anvil cell at GSECARS. *J. Synchrotron Radiat.* 12, 642–649. doi:10.1107/s0909049505022442

Shipley, A. M., Hutcheon, M. J., Needs, R. J., and Pickard, C. J. (2021). High-throughput discovery of high-temperature conventional superconductors. *Phys. Rev. B* 104, 054501. doi:10.1103/physrevb.104.054501

Shull, C., Wollan, E., Morton, G., and Davidson, W. (1948). Neutron diffraction studies of NaH and NaD. *Phys. Rev.* 73, 842–847. doi:10.1103/physrev.73.842

Skelton, J. M., Burton, L. A., Jackson, A. J., Oba, F., Parker, S. C., and Walsh, A. (2017). Lattice dynamics of the tin sulphides SnS2, SnS and Sn2S3: vibrational spectra and thermal transport. *Phys. Chem. Chem. Phys.* 19, 12452–12465. doi:10.1039/c7cp01680h

Somayazulu, M., Ahart, M., Mishra, A. K., Geballe, Z. M., Baldini, M., Meng, Y., et al. (2019). Evidence for superconductivity above 260 K in lanthanum superhydride at megabar pressures. *Phys. Rev. Lett.* 122, 027001. doi:10.1103/physrevlett.122.027001

Struzhkin, V. V., Kim, D. Y., Stavrou, E., Muramatsu, T., Mao, H.-k., Pickard, C. J., et al. (2016). Synthesis of sodium polyhydrides at high pressures. *Nat. Commun.* 7, 12267. doi:10.1038/ncomms12267

Toby, B. H., and Von Dreele, R. B. (2013). Gsas-ii: the genesis of a modern open-source all purpose crystallography software package. *J. Appl. Crystallogr.* 46, 544–549. doi:10.1107/s0021889813003531

Togo, A., and Tanaka, I. (2015). First principles phonon calculations in materials science. *Scr. Mater.* 108, 1–5. doi:10.1016/j.scriptamat.2015.07.021

Wang, H., Tse, J. S., Tanaka, K., Iitaka, T., and Ma, Y. (2012). Superconductive sodalite-like clathrate calcium hydride at high pressures. *Proc. Natl. Acad. Sci. U.S.A.* 109, 6463–6466. doi:10.1073/pnas.1118168109

Williams, W. L. (1962). Magnetic, thermal, and optical properties of the F center in NaH. *Phys. Rev.* 125, 82–86. doi:10.1103/physrev.125.82

Zha, C. S., Liu, Z., Ahart, M., Boehler, R., and Hemley, R. J. (2013). High-pressure measurements of hydrogen phase iv using synchrotron infrared spectroscopy. *Phys. Rev. Lett.* 110, 217402. doi:10.1103/physrevlett.110.217402

Zurek, E., Hoffmann, R., Ashcroft, N., Oganov, A. R., and Lyakhov, A. O. (2009). A little bit of lithium does a lot for hydrogen. *Proc. Natl. Acad. Sci.* 106, 17640–17643. doi:10.1073/pnas.0908262106